

# Cortical Magnification within Human Primary Visual Cortex Correlates with Acuity Thresholds

Robert O. Duncan\* and Geoffrey M. Boynton

Systems Neurobiology Laboratory - B  
The Salk Institute for Biological Studies  
10010 North Torrey Pines Road  
La Jolla, California 92037

## Summary

We measured linear cortical magnification factors in V1 with fMRI, and we measured visual acuity (Vernier and grating) in the same observers. The cortical representation of both Vernier and grating acuity thresholds in V1 was found to be roughly constant across all eccentricities. We also found a within-observer correlation between cortical magnification and Vernier acuity, further supporting claims that Vernier acuity is limited by cortical magnification in V1.

## Introduction

In primates, visual acuity is far better in the fovea than in the periphery. This bias is reflected by differences in spatial sampling between the fovea and periphery throughout early stages of visual processing; the sampling by the cone mosaic is approximately 40 times more dense in the fovea than in the periphery, and ganglion cells oversample foveal cones by a factor of four compared to the periphery (Curcio and Allen, 1990; Curcio et al., 1987). Emphasis toward the center of gaze is further exaggerated in the lateral geniculate nucleus (LGN) of the thalamus, where there are four times as many LGN cells per ganglion cell afferent in the fovea compared to the periphery (Connolly and Van Essen, 1984). Additionally, there are ten times more striate cells for every incoming LGN projection from the fovea (Connolly and Van Essen, 1984). Overall, there are approximately 160 times more striate cells per cone in the fovea than in the periphery. Thus, the surface area of primary visual cortex would have to be increased by a factor of roughly 13 ( $\approx\sqrt{160}$ ) to support peripheral sampling as fine as that of the fovea. This approximation is supported by retrograde labeling of the ganglion cell layer in macaques showing that ganglion cells near the fovea are allocated three to six times more cortical tissue than peripheral ones (Azzopardi and Cowey, 1993), a factor which increases to somewhere between 12 and 24 after the cone-to-ganglion cell ratio is taken into account. It therefore appears that the primate visual system has evolved toward a compromise whereby the infinitely dense visual array is sampled in a weighted fashion.

The traditional measure of this sampling process in the primary visual cortex (V1) is called the linear cortical magnification factor ( $M$ ), which is expressed in terms of millimeters of cortex per degree of visual angle (Daniel and Whitteridge, 1961).  $M$  is said to “match” visual acuity thresholds if  $M^{-1}$  scales with acuity thresholds. Because

cell density is roughly constant throughout V1 (Rockel et al., 1980), a match implies that the cortical representation of the minimally resolvable spatial distance is represented by a fixed number of V1 neurons, regardless of the eccentricity of the measurement.

Recently, estimates of  $M$  have been quantified in humans using fMRI (Engel et al., 1994, 1997; Sereno et al., 1995). However, it is not known if  $M$  matches acuity in individual observers because behavioral and anatomical data have yet to be compared in the same individuals. Accordingly, we used fMRI to determine  $M$  in V1, and we used two psychophysical tasks to measure acuity (Vernier and grating) in the same ten observers. Vernier acuity at a particular region of visual space is predicted to depend directly on  $M$  at a corresponding region within V1 in the contralateral hemisphere. Importantly, changes in Vernier acuity across the visual field should be represented by similar changes in the  $M$  of V1.

Across observers and the eccentricities tested, we found that a fixed distance in V1 closely represented threshold acuity. We also found a within-observer correlation between  $M$  and Vernier acuity but not between  $M$  and grating resolution. This second result further supports the idea that Vernier acuity is ultimately limited by the sampling resolution of V1.

## Results

One author (R.O.D.) and nine volunteers participated in our psychophysical and fMRI experiments. Participants were initially screened for normal acuity without optical correction using a Snellen eye chart. Informed consent was obtained in writing in accordance with guidelines established by the National Institutes of Health, and volunteers were paid for their time.

### Acuity Thresholds

We used two different stimuli and tasks to measure acuity. Vernier acuity stimuli were viewed binocularly on a computer monitor, while stimuli in a grating resolution task were viewed monocularly using laser interferometry. We chose a standard Vernier acuity task over other positional acuity measures, such as Landolt C's, two-point discrimination, and letter acuity, for two reasons. First, Vernier stimuli are frequently used by others to quantify visual acuity (Beard et al., 1997). Second, there is evidence to suggest that the Vernier acuity task is appropriate for exploring the cortical rather than the retinal limitations imposed on acuity (Levi et al., 1985). We chose to measure grating resolution with laser interferometry because this effectively circumvents the optics of the eye, and since it is not affected by individual differences in optical quality, it may afford a better measurement of the spatial resolution limit of the retinal image (He and MacLeod, 1996).

For the Vernier acuity task, horizontal Vernier stimulus offsets were measured using a two-alternative temporal forced-choice paradigm to obtain the threshold offset that resulted in 79% correct performance. Thresholds

\*Correspondence: rob@salk.edu

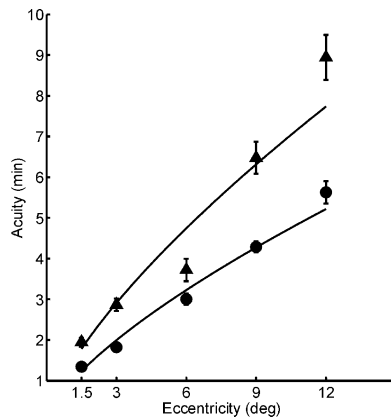


Figure 1. Mean Psychophysical Thresholds for All Ten Observers. Psychophysical thresholds are plotted as a function of the eccentricity from fixation. Triangles and circles denote mean thresholds in the grating resolution and Vernier acuity tasks, respectively. Error bars (when exceeding the size of the symbol) indicate the SEM. Solid lines represent the best-fitting power function to the results of each psychophysical task.

were obtained in each of the four visual quadrants for each observer at five eccentricities: 1.5°, 3°, 6°, 9°, and 12°. To minimize perceptual learning effects, subjects were given over an hour of pretraining, and the location of the psychophysical stimuli after training was randomized from session to session. These measures appear to be adequate; there were no systematic changes in Vernier or grating resolution thresholds between the first and second half of data collection (two-way ANOVA,  $p > 0.10$ ).

Psychophysical grating resolution was measured using a He-Ne laser interferometer. Interferometry was conducted on the University of California campus at San Diego according to a previously developed protocol (He and MacLeod, 1996). The interferometer introduces two point light sources that interfere with each other in the pupil plane so as to create a sinusoidal grating pattern directly on the retina. Stimuli were always presented at the same physical location, and the eccentricity of the stimulus relative to the center of gaze was determined by moving the fixation target with a stereotaxic apparatus. Gratings were presented at 1.5°, 3°, 6°, 9°, and 12° eccentricity to either the temporal- or nasal-inferior retina. The minimum angle of resolution (MAR) was determined for each eccentricity using a staircase procedure. We measured the maximum spatial frequency for which each observer could determine (at 79% correct) the direction of a 15° shift in grating orientation from horizontal.

Mean psychophysical thresholds for all ten observers are plotted as a function of the eccentricity of the stimulus (Figure 1). Triangles denote thresholds for the grating resolution task, and circles denote thresholds for the Vernier acuity task. Each point represents a mean threshold for all measured hemifields and all observers. For the Vernier acuity task, four repetitions from each quadrant (eight from each hemifield) were averaged to yield mean thresholds for each eccentricity. For the grating resolution task, means were computed by averaging one threshold from each hemiretina (e.g., left eye temporal retina and right eye nasal retina). Mean thresholds

for the grating resolution task are expressed as the period (in minutes of visual angle) of the grating at threshold. Error bars indicate one SEM. For all ten observers, mean thresholds increase with increasing eccentricity. The solid lines represent the best fits to the Vernier and grating resolution data, described by the power functions  $\tau = 0.93 \times \delta^{0.69}$  and  $\tau = 1.34 \times \delta^{0.71}$ , respectively, where  $\tau$  is threshold, and  $\delta$  is eccentricity. As indicated by the similar exponents in the power function fits, Vernier acuity did not decline any faster than grating acuity as a function of eccentricity. This small discrepancy between our data and an earlier study (Levi et al., 1985) may have been the result of not collecting thresholds from the fovea, where Vernier and grating acuity differ the most. Alternatively, it may also have been because our grating acuity measurements were not affected by the optics of the eye.

### Measurements of Cortical Magnification

Blood oxygenation-level dependent (BOLD) functional magnetic resonance imaging (fMRI) was used to measure  $M$  in the same ten observers. First, a high-resolution ( $1 \times 1 \times 1$  mm) anatomical volume of the brain was obtained using an MPRAGE pulse sequence. Next, standard retinotopic mapping stimuli were applied to localize V1 (Engel et al., 1994; Sereno et al., 1995). Finally, a series of functional scans were used to localize the cortical area devoted to a particular eccentricity of visual space.

Previous fMRI studies have measured  $M$  in humans by using the temporal phase of the fMRI response to expanding and contracting rings (Engel et al., 1994, 1997; Sereno et al., 1995; Smith et al., 2001). Cortical magnification of the fovea predicts that changes in the temporal phase of the fMRI response should accelerate as the stimulus moves at a constant rate from the fovea to the periphery. Unfortunately, it is difficult to determine the exact temporal phase that corresponds to the fovea, because the expanding rings wrap around from the periphery back onto the fovea. Furthermore, the cortical representation of the extreme periphery is underestimated due to the lack of visual stimulation beyond the greatest eccentricity of the stimulus as it wraps around to the fovea. As a consequence, the temporal phase tends to decelerate toward the furthest peripheral position measured, which incorrectly implies increasing  $M$  with eccentricity.

To obtain a more accurate estimate of  $M$ , we used a combination of conformal mapping techniques and stimuli made from stationary flickering annuli. Annuli composed of counterphase-modulated checkerboard patterns (mean luminance, 340 cd/m<sup>2</sup>; contrast, 100%; 8 Hz) had radii of 1.5°, 3°, 6°, 9°, or 12° of visual angle (determined as the average of outer and inner radii). Observers were instructed to fixate a target ( $0.25^\circ \times 0.25^\circ$ ) positioned at the center of the screen, while one of the five rings was presented surrounding the center of gaze. The thickness of each ring was roughly 1/6 of the eccentricity. Note that each of the five rings may stimulate a different amount of cortex, but differences in the amount of cortex activated should not profoundly affect the mean location of activity on the flattened cortex. In a single session, a ring with a given eccentricity was presented in alternation with a mean luminance

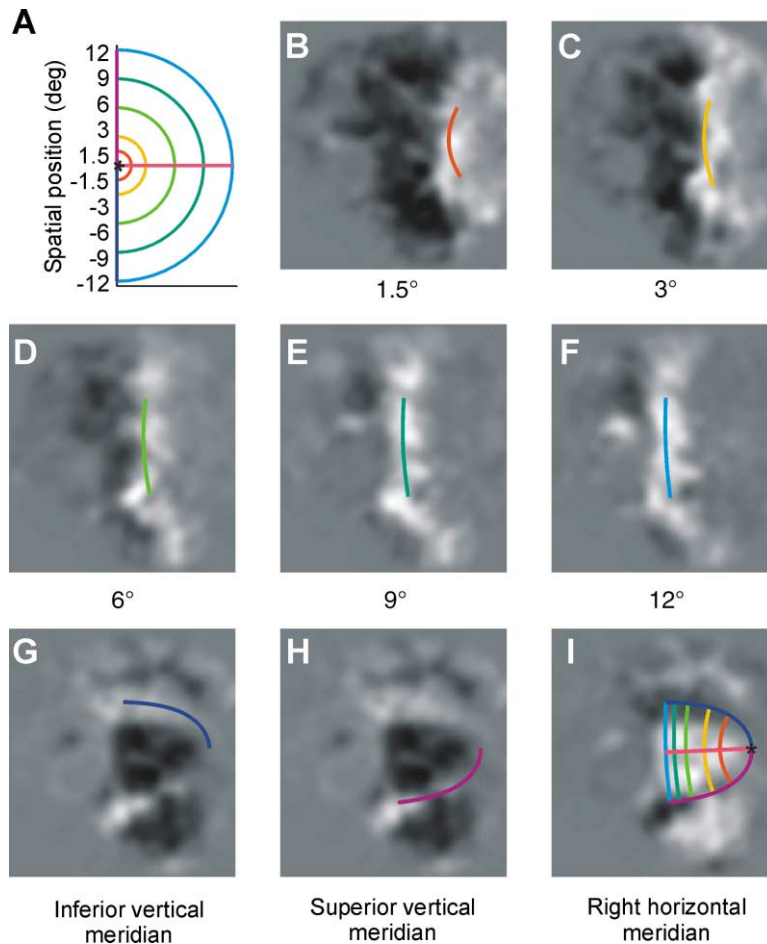


Figure 2. fMRI Results for a Single Observer (A) Schematic representation of our stimuli in polar coordinates for one hemifield. The colored arcs represent the location and eccentricity of flickering annuli, relative to the fixation target (asterisk). Vertical and horizontal meridians were also mapped with flickering wedges, and the location of these stimuli are also color coded. (B–I) The remaining fMRI images are from the brain hemisphere contralateral to the visual hemifield in the upper left panel. All images are from the same observer (R.O.D.), and the computational flattening for each image is identical. Bright pixels correspond to increased BOLD signal that correlates with the stimulus time course. (B–F) Brain images correspond to the five flickering annuli (1.5°, 3°, 6°, 9°, and 12° eccentricity). Superimposed colored arcs represent the projection (based on a single, best-fitting template) of the annulus of matching color in (A). (G and H) Activity for inferior and superior vertical meridians, respectively. (I) Activity for the horizontal meridian along with a single, best-fitting template for the entire data set.

screen for 6 1/2, 40 s cycles. Data from the first 1/2 cycle was discarded to avoid magnetic saturation effects.

A map of activity representing the fMRI response to each stimulus was calculated by correlating the time course of the fMRI response from each voxel with a sinusoid of the stimulus frequency (40 s period). The resulting correlations and temporal phases were then projected onto a unit vector representing the expected temporal phase of the response (based on the typical hemodynamic delay). This map was projected onto the computationally flattened representation of each observer's occipital lobe.

The resulting activity maps in the flattened representation of the cortex appear as distinct patterns that vary systematically with the eccentricity of the stimulus (Figure 2). The upper left panel (Figure 2A) shows a schematic representation of our stimuli for one hemifield of visual space. Each arc represents the location and eccentricity of our annulus relative to the fixation target (asterisk). Note that, while all of our stimuli were complete annuli, only the portion that extends into the right hemifield is presented here for clarity. Each eccentricity is coded by a differently colored arc. The vertical and horizontal meridians are also color coded, and each of these lines represents the primary axis of stimulation by our meridian-mapping stimuli. The grayscale images in the remaining panels (Figures 2B–2I) show fMRI activity maps on flattened representations of one observer's left

occipital cortex. Each image shows a unique pattern of activity associated with a different member of our stimulus set. Bright pixel values correspond to changes in BOLD signal that correlate positively in time with the stimulus presentation. Figures 2B–2F show patterns of fMRI activity to each of the five flickering annuli. Figures 2G–2I show the pattern of activity produced while viewing stimuli presented in the horizontal and vertical meridians.

To describe the topology of a given observer's V1, we fit these fMRI activity maps with a template derived from a conformal mapping method developed by Schwartz (1980, 1994). According to Schwartz, two-dimensional visual space can be projected onto the two-dimensional flattened cortex using the formula  $w = k \times \log(z + a)$ , where  $z$  is a complex number representing a point in visual space, and  $w$  represents the corresponding point on the flattened cortex. The parameter  $a$  reflects the proportion of V1 devoted to the foveal representation, and the parameter  $k$  is an overall scaling factor. We added an additional parameter,  $b$ , to scale the width of the map. To achieve this, we separated the real and imaginary components of our projected positions,  $w$ , and scaled the real component by parameter  $b$ . This modification affords better fits by sacrificing the preservation of local isotropy.

The best-fitting template for each hemisphere in each observer was obtained by projecting a curve representing the location of the visual stimulus onto the correspond-

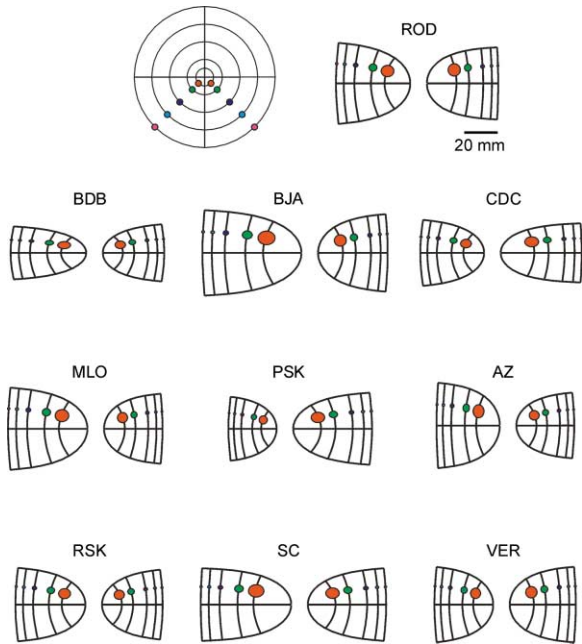


Figure 3. Templates for V1 in Both Hemispheres and All Ten Observers

(Upper left) Schematic denoting the location of the 1° diameter patches of visual space. Each eccentricity is marked with a unique color. (Remaining panels) Individual, best-fitting templates for each hemisphere in our ten observers. Corresponding projections of visual space onto the flattened representation are indicated by color.

ing fMRI activity map and then adjusting parameters to maximize the image intensity (i.e., the line-integral) under the projected curve. Parameter values from the best-fitting template were obtained using a nonlinear optimization technique in MATLAB. The optimized fits for a single observer are superimposed upon the grayscale activity maps in Figure 2. As the radius of the presented annulus increases, the arc-shaped pattern of activation moves gradually from the fovea to the periphery in the flattened representation of the cortex (Figure 2B–2F). The colored lines superimposed upon the patterns of activity show the locations, projected using parameters from the best-fitting template, of the corresponding annuli and meridian-mapping stimuli (Figure 2B–2I). Each component is color coded to match the scheme in Figure 2A. Superimposed upon the pattern of activity in the last panel (Figure 2I) is the best-fitting template for all stimuli (including the fit for the horizontal meridian).

A single, best-fitting template computed for each observer's hemisphere is shown in Figure 3, with the template from Figure 2 replotted in the upper right panel. There is a noticeable difference in overall V1 area both within observers (the smaller hemisphere being as little as 46% of the larger in the most asymmetric observer) and between observers (ranging from 418 to 1131 mm<sup>2</sup>, the smallest hemisphere being 37% of the largest). This 2.7 factor variation between individuals is similar in magnitude to previous results reported in humans (Filimonoff, 1932; Sholl, 1956; Stensaas et al., 1974) and macaques (Van Essen et al., 1984).

For each hemisphere and eccentricity,  $M$  can be com-

puted by first using the best-fitting template to project a 1° diameter patch of visual space onto the flattened cortex and then calculating the diameter of the resulting cortical projection. The colored patches superimposed upon each template within Figure 3 are the resulting cortical projections at the five eccentricities shown in the upper left panel. Each eccentricity is marked with a unique color. The area of cortex devoted to the fovea is clearly exaggerated relative to the periphery for all hemispheres. This trend is maintained despite the large within-observer and between-observer variability in the size of V1.

We independently fit five templates to each hemisphere to obtain an error estimate for the fitting procedure itself. Each initial condition was chosen by eye, and then the parameters (offset, rotation,  $a$ ,  $b$ , and  $k$ ) were optimized using MATLAB's nonlinear optimization routines. Each of the five templates that were fit to the fMRI data was used to project 1° patches of visual space onto the flattened representation of the cortex. The projected areas generated from each template were then used to compute a mean projected area and confidence intervals for each eccentricity. A final estimate of  $M$  was derived from the averaged cortical projections.

The starting point for each template in our fitting procedure was first computed automatically using our software and then adjusted manually by the experimenter. First, we determined the center of activity for fMRI responses to our most foveal stimulus (1.5°) and moved the origin of the template to that location. Second, we computed the center of mass for fMRI responses to our most peripheral stimulus (12°). The angle of the line segment connecting these two points was computed, and the horizontal meridian of the template was rotated to this angle with its origin fixed. All the other parameters in the template ( $a$ ,  $b$ , and  $k$ ) were set to default values that roughly corresponded to an average V1 size across subjects. If necessary, we adjusted the output of this initial automatic fitting procedure to obtain the closest fits possible by visual inspection. After any manual adjustments were complete, the template was fit to the data using the iterative method described above. The order in which each hemisphere was fit was randomized to avoid starting each of the five fits for each hemisphere from the same seed (i.e., using the same parameters).

The open circles in Figure 4 show the calculated value of  $M$  for each of five eccentricities in both hemispheres, averaged across all ten observers. As expected, regions representing foveal vision are associated with a greater  $M$  than regions devoted to the periphery. The line through the open circles in Figure 4 shows the power function fit  $M = 9.81 \times \delta^{-0.83}$ , where  $\delta$  denotes eccentricity.

### Comparing Acuity to Cortical Magnification

We compared psychophysical thresholds directly to  $M$  for all observers (Figure 5). Mean thresholds for both acuity tasks are plotted as a function of mean  $M$  on log-log axes. The symbol shape of the data point denotes the eccentricity of each stimulus. Open symbols denote values for the grating resolution task, and closed symbols represent values for the Vernier task. Acuity thresholds are smallest near the fovea, where cortical magnifi-

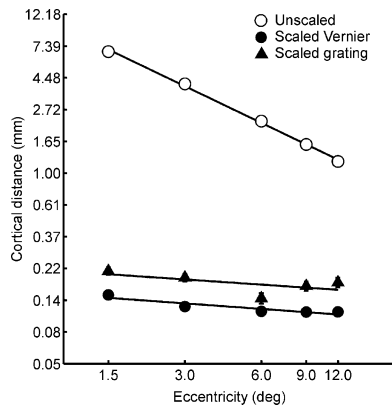


**Figure 4. Cortical Distance as a Function of Eccentricity**  
Each brain hemisphere was fit with a template five times, and each template was used to compute an individual estimate of  $M$  for that hemisphere. The value of  $M$  was obtained by projecting  $1^\circ$  diameter patches of visual space onto the flattened representation of V1, using each template. Computed  $M$  for each eccentricity was averaged across five repeats (for each of the five fits) to yield a better estimate of  $M$  for each brain hemisphere. (Open circles) Data points represent computed  $M$  averaged across 20 hemispheres at a given eccentricity. Error is plotted as the SEM for all 20 hemispheres, which is smaller than the marker icon. The straight line indicates the best-fitting power function to the data. (Closed symbols) Patches of visual space with a diameter determined by the psychophysical thresholds at each eccentricity were projected onto cortex using the techniques described above. Circles and triangles indicate projections scaled by Vernier thresholds and grating resolution thresholds, respectively. With scaling, the resulting cortical projections are roughly equivalent across eccentricity.

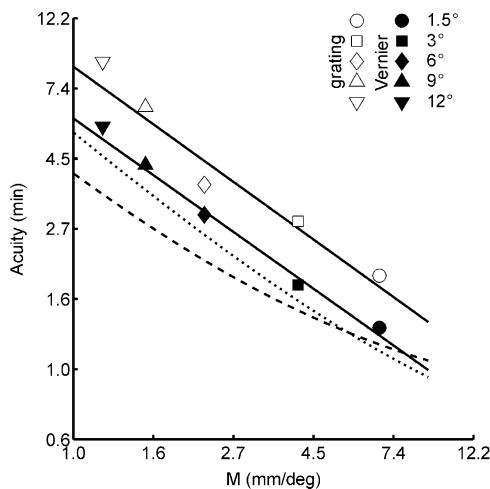


**Figure 5. Psychophysical Thresholds versus  $M$**   
Mean psychophysical thresholds on the grating resolution task (open symbols) and the Vernier acuity task (closed symbols) are plotted as a function of projected cortical diameter. Data points represent mean  $M$  and mean psychophysical threshold across all observers. Error bars for these mean values were previously plotted in Figures 1 and 4. Symbol shape indicates eccentricity. Solid lines denote the best power fit to our data, which roughly equates acuity with the inverse of  $M$ . Dotted lines describe the best-fitting power function relating Popovic and Sjostrand's psychophysical data (Popovic and Sjostrand, 2001) to the fMRI data set of Engel and colleagues (Engel et al., 1997). (Dashed line) The best-fitting power function relating Popovic and Sjostrand's psychophysical data to the fMRI data set of Sereno et al. (Sereno et al., 1995).

cation is largest. This relationship can be described by the power functions  $\tau_{\text{VERNIER}} = 5.97 \times M^{-0.81}$  and  $\tau_{\text{GRATING}} = 8.63 \times M^{-0.82}$ , where  $\tau$  denotes the mean threshold. An exponent of  $-1$  means that acuity thresholds are roughly inversely proportional to  $M$  across eccentricity. The correlation coefficient ( $r$ ) for grating resolution and  $M$  is  $-0.85$ , and  $r$  for Vernier acuity and  $M$  is  $-0.93$ . Correlation coefficients were computed for the entire population of observers rather than for the average across observers. The difference between these two coefficients is not significant ( $p > 0.10$ ). The slopes of these functions ( $-0.81 \pm 0.06$  for Vernier;  $-0.82 \pm 0.10$  for grating) are significantly different from both  $-1$  and  $0$ . Additional testing of the fits generated by simple linear regression (SLR) indicates that the slopes are not different from each other. Even though a significant difference exists between the elevations of the slopes ( $p < 0.05$ ), differences in elevation do not address the question at hand; different tasks are expected to have differences in absolute thresholds at each eccentricity.

Another way to illustrate the close relationship between acuity and  $M$  in V1 is to calculate the amount of visual cortex that represents a circular patch of visual space having a diameter equal to each observer's acuity threshold. For the Vernier acuity task, we set the diameter of the patch to the mean horizontal separation between lines at threshold. For the grating resolution task, the patch diameter was set to the mean period of the grating at threshold. The amount of cortex representing a threshold stimulus was averaged across all hemispheres and observers and is plotted in Figure 4. Closed triangles correspond to the grating resolution task, and closed circles correspond to the Vernier acuity task. Remarkably, the computed cortical distance is roughly constant across the eccentricities tested, which indicates that a constant distance in the cortex represents the physical space occupied by all acuity thresholds (0.12 mm for Vernier and 0.18 mm for grating resolution). The slopes for both acuity measurements (approximately  $-0.13$ ) are significantly different from zero (both  $p < 0.05$ ) but small relative to the slope for the unscaled data (approximately  $-0.83$ ). The residual slopes after scaling are predicted by single-unit physiology (Dow et al., 1981); when the acuity data of Weymouth et al. (1928) was projected onto the cortex using  $M$ , there was a slight negative slope as well. Dow and colleagues found that acuity thresholds instead scale proportionately with the "point image" on V1. The point image was taken to be  $M \times F$ , where  $M$  is cortical magnification and  $F$  is the aggregate receptive field size (a combination of receptive field size and receptive field overlap). Receptive field (RF) overlap is known to increase as one moves closer to the fovea (Dow et al., 1981). For both our study and that of Weymouth and colleagues, psychophysical thresholds are greater than what is predicted by  $M$  near the fovea, which may be the result of the increase in RF overlap with decreasing eccentricity.

Given the strong relationship between  $M$  and psychophysical thresholds across eccentricity, we might expect to find a within-observer correlation between  $M$  and psychophysical thresholds. The results of this comparison for grating resolution and Vernier acuity tasks

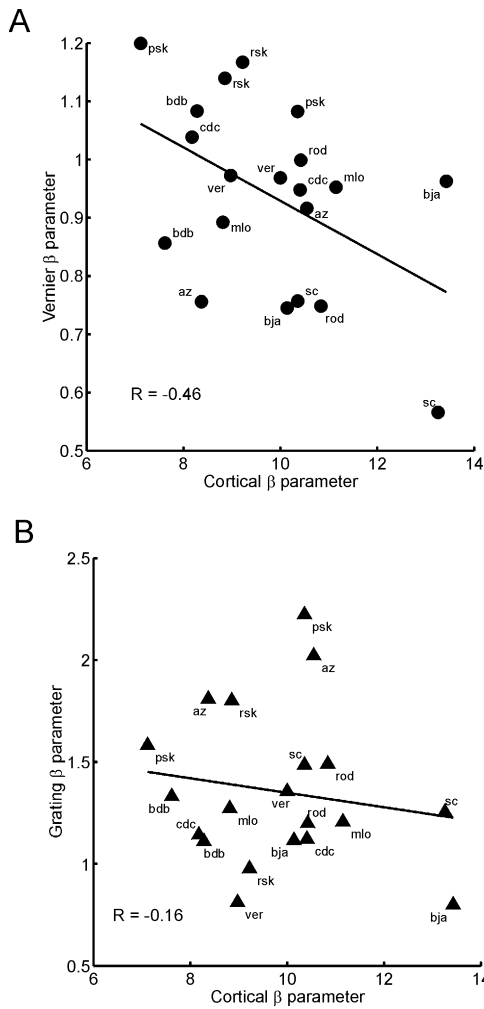


Figure 6. Within-Observer Comparison between Overall  $M$  and Overall Psychophysical Thresholds

A comparison was made between  $M$  and acuity thresholds for each hemisphere/hemifield of each observer. First, changes in  $M$  with eccentricity and changes in psychophysical thresholds with eccentricity were individually fit with the power function  $y = \beta \times x^p$ . Then, the  $\beta$  parameters for  $M$  and the psychophysical data sets were correlated.

(A) The  $\beta$  parameters for Vernier acuity thresholds are plotted as a function of the  $\beta$  parameters for  $M$ .

(B) The  $\beta$  parameters for grating resolution thresholds are plotted as a function of the  $\beta$  parameters for  $M$ . There is a significant correlation between  $\beta$  parameters for  $M$  and  $\beta$  parameters for Vernier acuity but not for grating resolution.

are plotted in Figures 6 and 7. For each subject, the change in  $M$ , grating resolution thresholds, and Vernier acuity thresholds across eccentricity for each hemifield/hemisphere were fit with power functions:  $y = \beta \times \delta^p$ , where  $\delta$  is eccentricity, and  $y$  is either threshold or  $M$ . The parameter  $\beta$  represents the  $y$  intercept for each function on log-log axes or, equivalently, the estimated acuity, or  $M$  at  $1^\circ$  of eccentricity. The parameter  $\beta$  can be thought of as an overall scale factor for each power function fit. We predicted that hemispheres with large  $\beta$  parameters for  $M$  should have smaller  $\beta$  parameters for psychophysical thresholds and vice versa, indicating

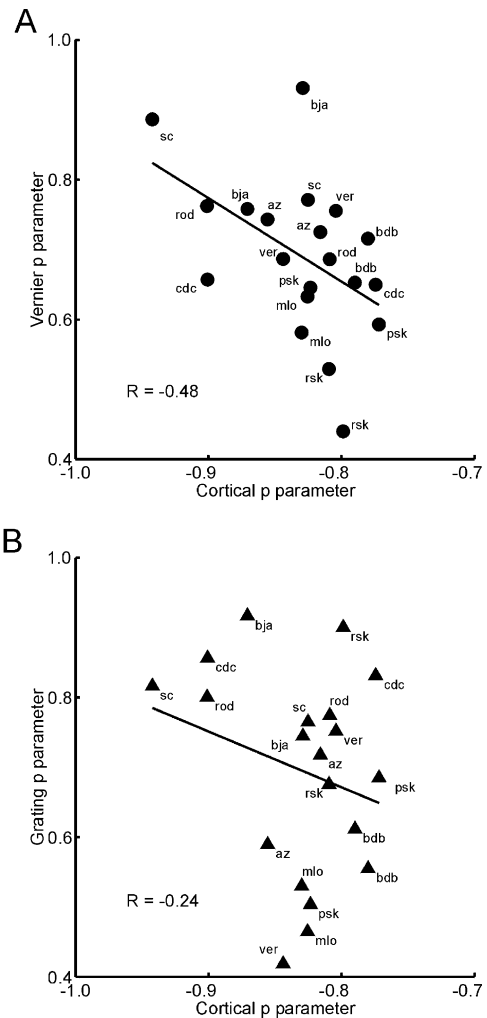


Figure 7. Within-Observer Comparison between the Change in  $M$  and the Change in Psychophysical Thresholds

Changes in  $M$  with eccentricity and changes in psychophysical thresholds with eccentricity were individually fit with the power function  $y = \beta \times x^p$ .

(A) The  $p$  parameters for Vernier acuity thresholds are plotted as a function of the  $p$  parameters for  $M$ .

(B) The  $p$  parameters for grating resolution thresholds are plotted as a function of the  $p$  parameters for  $M$ . There is a significant correlation between  $p$  parameters for  $M$  and  $p$  parameters for Vernier acuity. The change in  $M$  predicts the change in Vernier acuity thresholds with eccentricity, but there is not enough evidence to prove this relationship exists between  $M$  and grating resolution.

better overall visual acuity for subjects with overall larger cortical magnification factors. We found a significant within-hemisphere/hemifield negative correlation ( $r = -0.46, p < 0.05$ ) between  $\beta$  parameters for  $M$  and Vernier acuity thresholds (Figure 6A). We did not, however, find a significant within-observer correlation between the  $\beta$  parameters for grating resolution thresholds and  $M$  ( $r = -0.16, p > 0.05$ ) (Figure 6B). There was no significant difference between the correlations for Vernier acuity and grating resolution ( $p > 0.10$ ).

Correlating the  $p$  parameters provides a comparison between the change in psychophysical thresholds to the change in  $M$  with increasing eccentricity, after ac-

counting for overall scale factors. Correlations between the  $p$  parameters for Vernier acuity and  $M$  (Figure 7A) were significant ( $r = -0.48$ ,  $p < 0.05$ ). This means that subjects with the most rapid increase in Vernier acuity thresholds with eccentricity also have the most rapid decrease in cortical magnification with eccentricity. By contrast, correlations between the  $p$  parameters for grating resolution and  $M$  (Figure 7B) were not significant ( $r = -0.24$ ,  $p > 0.10$ ). We did not find a significant difference between these two correlations ( $p > 0.10$ ).

We tested the reliability of the correlations (for  $\beta$  or  $p$ ) using each of the five independent fits to the fMRI data. Five of the ten comparisons (five repeats for  $\beta$  or  $p$  parameters) between Vernier acuity and  $M$  were significant. Finding correlations of this magnitude for *both* parameters is extremely unlikely by chance. We calculated the likelihood of observing our correlation values by performing a Monte Carlo simulation in which the association between measurements of acuity and  $M$  were randomly shuffled across subjects. That is, each of the 20 curves showing the effects of Vernier acuity with eccentricity (ten subjects  $\times$  two hemispheres) was randomly associated with one of the 20 curves representing  $M$ . For each random association, we calculated the  $\beta$  and  $p$  parameters. The probability that a random association between acuity thresholds and  $M$  has correlations for  $\beta$  and  $p$  parameters that are more extreme than our observed correlations is less than 1 in 250. Hence, while the correlations between  $p$  parameters for Vernier acuity and  $M$  are moderate, we believe they reflect a real within-observer correlation between Vernier acuity and  $M$ .

We have taken precautions to assure that the correlations reported are not heavily influenced by outliers. Tests for homogeneity of variance were conducted to ensure the assumptions of regression were met. For the cases where outliers did exist, we performed a robust weighted regression (iterative bisquare weighted regression). The correlations were also tested without the outliers. All of the correlations that tested positive for heteroscedacity were still significant after taking these precautions (all  $p < 0.05$ ).

## Discussion

### Summary

We report two main findings. First, power function fits to the relationship between  $M$  in V1 and acuity show exponents of about  $-0.85$  for both acuity tasks across subjects. This value is close to  $-1$ , which indicates a close match between acuity thresholds and spatial sampling in V1. Correspondingly, scaling patches of visual space by observers' psychophysical thresholds results in roughly equal-sized cortical projections on the flattened representation. This result implicates V1 as a limiting factor for human visual acuity because it implies that the cortical representation of the minimally resolvable spatial distance is represented by a fixed number of V1 neurons, regardless of the eccentricity of the measurement.

Nevertheless, the match between visual acuity and  $M$  is not perfect; foveal acuity thresholds are slightly higher than predicted by  $M$  at the fovea. This is made evident

by the fact that the exponent of the power function fits to the relationship between  $M$  and acuity is greater than  $-1$  and that scaled acuity thresholds projected onto V1 (Figure 4, closed symbols) cover more cortical distance for the more foveal stimuli. Previous comparisons of acuity and  $M$  also demonstrate this result, which has been attributed to greater receptive field overlap at the fovea (Dow et al., 1981). It has been recently demonstrated that RF size can be predicted by areal cortical magnification (ACMF) to the  $-2/3$  power (Stevens, 2002). The exponent in this equation is greater than  $-1$  because RF size does not decrease as fast as inverse ACMF with decreasing eccentricity, which implies that RF overlap increases at the fovea. The greater overlap near the foveal representation may be the result of an anatomical constraint on the minimum size of a cell's receptive field. Until now, it has been unclear whether RF overlap would lead to an increase or decrease in acuity thresholds (Dow et al., 1981). By finding an increase in parafoveal acuity thresholds relative to what is predicted by ACMF, we support the hypothesis that increased receptive field overlap results in relatively poorer visual acuity.

Our second finding is that observers with larger overall cortical area in V1 had lower overall Vernier acuity thresholds. Additionally, we found that subjects showing greater changes in  $M$  with eccentricity also had greater changes in Vernier acuity thresholds with eccentricity. Approximately 21%–23% of the variability in Vernier thresholds across observers can be attributed to differences in cortical topology. While this correlation does not necessarily imply causality, this result along with our first finding further implicates V1 as a limiting factor in Vernier acuity.

On the other hand, we did not find a significant correlation between individual acuity thresholds and cortical magnification for the grating resolution task. One possible explanation for this is that there was more variability in the grating acuity threshold measurements. This variability may be due to the relatively unnatural viewing conditions associated with laser interferometry (i.e., monocular viewing and speckle artifacts) compared to the Vernier acuity task. Alternately, one post-hoc explanation for the lack of correlation between  $M$  and grating acuity is that the visual cortex of an individual may have developed to match the quality of the optical image, as measured by Vernier acuity, rather than matching the actual sampling of the retina, which can be measured independent of the optics using interferometry.

### Prior Investigations of Acuity and $M$

Previous studies show that grating resolution matches cone and ganglion cell sampling density (Rolls and Cowey, 1970), while Vernier acuity thresholds more closely match cortical magnification in V1 (Dow et al., 1981). Our results, however, show that *both* grating acuity and Vernier acuity thresholds roughly match sampling in V1. Two possible reasons for our finding with grating resolution are (1) previous studies did not present gratings using laser interferometry, and (2) we only measured grating resolution down to  $1.5^\circ$  of eccentricity, and the largest differences between Vernier and grating acuity appear with foveal presentation (Levi et al., 1985; Westheimer, 1982).

Visual processing does not end in V1; it is likely that extrastriate visual areas also have cortical magnification factors that match acuity thresholds. Pursuing this notion is indeed one of our long-term goals, but our ability to address this question has been limited by practical considerations. Our complex-log map is only appropriate for describing the topology of V1. The computational algorithm for achieving this task is simple yet powerful. Unfortunately, we do not yet know of such a simple map for describing the topology of the four separate maps of area V2 or for higher visual areas.

Our psychophysical and  $M$  results compare favorably to those measured in previous studies. A common parameter that characterizes the increase in acuity thresholds in the periphery is  $E_2$ , which is the eccentricity at which foveal thresholds double (Levi et al., 1984, 1985). In a meta-analysis of 23 studies using different Vernier stimuli, values of  $E_2$  averaged  $1.5^\circ$ , with a range from  $0.07^\circ$  to  $20^\circ$  (Beard et al., 1997). Despite the simplicity of this descriptive statistic, the large variance between studies demonstrates that  $E_2$  is quite task specific. Consequently, the validity of using  $E_2$  as a reliable measure to infer cortical magnification has since been called into question (Whitaker et al., 1992). Furthermore, estimates of  $E_2$  depend heavily on contrast sensitivity (Levi et al., 2000), and thus, attempts to reconcile our psychophysical results with the literature may not be entirely possible at this time. Even though we did not collect psychophysical data from the fovea, we can estimate  $E_2$  by first fitting our psychophysical data with a power function and then extrapolating the fit to the fovea. We report an  $E_2$  of  $1.34^\circ$ , which is very close to the mean  $E_2$  across studies reported by Beard et al. (1997) and within the limits provided in Levi et al. (2000).

There are very few investigations of grating resolution in the periphery using laser interferometry. Those that measure acuity in the fovea (e.g., He and MacLeod, 1996) find maximal resolution approaching 60 cpd. Some grating *detection* tasks preserve acuity thresholds as high as 30 cpd beyond  $20^\circ$  in the periphery (Coletta and Williams, 1987; Thibos et al., 1987). However, grating *resolution* tasks like the one employed in the current study tend to elicit thresholds closer to those obtained without interferometry. Our mean grating resolution thresholds range from 31 to 7 cpd between  $1.5^\circ$  and  $12^\circ$  in the periphery. Similar to our results, the grating acuity thresholds of Kerr (1971), Thibos et al. (1987), and Wertheim (1894) are all around 30 cpd near  $1.5^\circ$  eccentricity. Furthermore, grating acuity thresholds from Kerr (1971) and Thibos et al. (1987) fall to around 10 cpd at  $12^\circ$  eccentricity, while the data of Wertheim is closer to 6 cpd. Clearly, our data are very similar. We report an  $E_2$  of  $1.9^\circ$  for our grating resolution measurements.

We compared our measurements of  $M$  with the measurements of others. The eccentricity at which inverse  $M$  doubles, also referred to as  $E_2$ , was first determined for our data. The resulting  $E_2$  ( $\sim 0.76^\circ$ ) corresponds nicely to well-established measurements of  $E_2$  (ranging from  $0.77^\circ$  to  $0.97^\circ$ ) obtained from macaques (Dow et al., 1981; Tootell et al., 1982; Van Essen et al., 1984). Directly measuring  $M$  in humans is difficult, and, as a consequence, there is little cortical magnification data collected in humans. Brindley and Lewin (1968) implanted an array of electrodes into the occipital cortex of a 52-

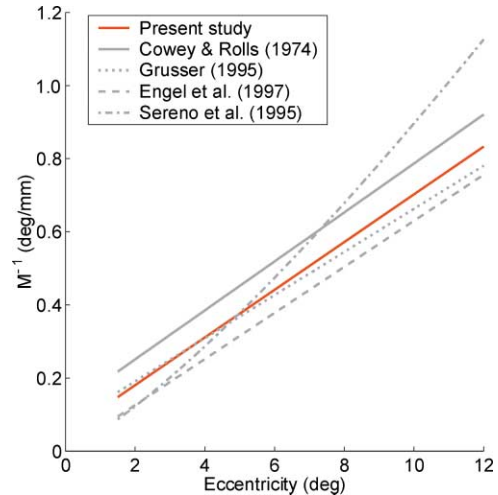


Figure 8. Independent Measurements of  $M$  in V1

We plotted inverse  $M$  as a function of eccentricity for this study alongside the measurements made by several other studies in humans (Covey and Rolls, 1974; Engel et al., 1994; Grusser, 1995; Sereno et al., 1995). It is refreshing to see that estimates of the relationship between  $M$  and eccentricity are quite similar across independent investigations using widely varying techniques. Measurements of  $M$ , however, appear larger near the fovea for the other fMRI paradigms (Engel et al., 1994; and Sereno et al., 1995). The other fMRI studies estimated  $M$  using flickering annuli that expanded from the fovea to the periphery and then wrapped around back onto the center of gaze, which may have made it difficult to accurately estimate  $M$  at the fovea. For Sereno and colleagues,  $M$  might be underestimated in the periphery for the same reason.

year-old patient suffering from severe glaucoma. By inducing a mild current through the array, the authors could record a retinotopic map of the phosphenes perceived by the patient. Covey and Rolls (1974) later used this data to compute the cortical magnification factor in humans. The linear relationship between  $1/M$  and eccentricity could be described by the equation  $1/M = 0.067E + 0.117$  (as described by Grusser, 1995). We plotted this data alongside ours ( $1/M = 0.065E + 0.054$ ) for comparison (Figure 8). The two estimates of  $M$  agree quite closely. Another creative study (Grusser, 1995) measured  $M$  by tracing the phosphenes evoked during migraine headaches. The authors characterized their results using the equation  $1/M = 0.059E + 0.073$ , which also agree quite closely with our estimate.

Recently, estimates of  $M$  have been acquired using fMRI. Estimates of  $M$  are obtained from subjects who passively view expanding and/or contracting annuli composed of flickering checkerboard patterns. These stimuli produce a traveling wave of activity across the flattened representation of the cortex. The temporal phase of the activity reflects the stimulus position in the visual field. Fitting this temporal phase as a function of cortical distance can provide a measure of  $M$  (Engel et al., 1994). Sereno et al. (1995) estimated the  $M$  using the formula  $M = 20.5(E + 0.08)^{-1.26}$ . Similarly, Engel et al. (1997) found an exponential function  $E = \exp(0.063(d + 36.54))$ , where  $d$  is the cortical distance in millimeters, and  $E$  is the visual field eccentricity in degrees. This equation reduces to  $M = 15.87/E$  (Popovic and Sjostrand, 2001). These functions are all also plotted along-

side our data (Figure 8). It is encouraging to find these measurements of  $1/M$  are in close agreement. However,  $M$  is larger near the fovea for Engel and Sereno, which may be overestimated because of stimulus wraparound in their paradigm. Likewise, Sereno's data might be underestimated in the periphery for the same reason.

Our study directly compares  $M$  and visual acuity in the same human individuals, in contrast to previous comparisons of psychophysics to  $M$  (e.g., Levi et al., 1985; Rovamo et al., 1978) that borrowed independent measurements of  $M$  from nonhuman primates (e.g., Daniel and Whitteridge, 1961; Dow et al., 1981) or from humans (e.g., Brindley and Lewin, 1968; Cowey and Rolls, 1974). For example, Popovic and Sjostrand (2001) recently compared independent estimates of acuity thresholds (MAR), ganglion cell separation (S), and  $M$  in humans obtained with fMRI. They found similar results to those reported here; visual acuity was linearly related to  $M^{-1}$ . The slope of the line relating  $M^{-1}$  varied slightly as a function of the fMRI data set. For the Engel et al. data set (Engel et al., 1997)  $M^{-1} = 0.2 \times \text{MAR} - 0.08$ , and for the Sereno et al. data set (Sereno et al., 1995)  $M^{-1} = 0.3 \times \text{MAR} - 0.21$ . In comparison, the slopes of the lines relating  $M^{-1}$  to acuity thresholds for our two tasks were  $M^{-1} = 0.13 \times \text{MAR} + 0.03$  for Vernier acuity and  $M^{-1} = 0.07 \times \text{MAR} + 0.11$  for grating resolution. We plotted Popovic and Sjostrand's analysis of the Engel et al. data (Figure 5, dotted line) and the Sereno et al. data (Figure 5, dashed line) alongside ours. Differences in the elevation of the fits are likely due to differences between our psychophysical paradigm and theirs. Nevertheless, the linearity of the fits supports the notion that acuity is represented by a fixed distance in V1.

#### Within-Observer Differences and Implications for Amblyopia

Given their close relationship, we predict Vernier acuity and  $M$  should covary under a variety of circumstances. One might expect nasotemporal differences in monocular acuity to be reflected by  $M$  in V1. Although there is a nasal bias for acuity in the far periphery (Fahle and Schmid, 1988), there is little nasotemporal asymmetry within the central  $10^\circ$  (Wilhelm and Fahle, 1993). When more peripheral stimuli are viewed, we predict  $M$  should closely parallel the better acuity of the nasal hemiretina. In our study, we only looked at the central  $12^\circ$ , and therefore, we would not expect to find a nasotemporal asymmetry. We were also unable to directly test this prediction because our Vernier stimuli were viewed binocularly. We did, however, test to see if there was a difference between dorsal and ventral  $M$  in V1 that correlated with Vernier acuity in the superior and inferior visual hemifields. We fit the dorsal and ventral portions of V1 separately for each hemisphere by fixing the position and rotation of the conformal map while fitting the other parameters. We did not find a difference between the correlations for  $M$  and acuity when comparing the Vernier thresholds to  $M$  for upper and lower visual fields ( $p > 0.10$ ). This lack of a finding is probably due to the lack of a significant difference between the acuity for targets in the upper versus lower visual fields ( $p > 0.10$ ).

For patients with amblyopia, the relationship between  $M$  and acuity is less obvious. While the retina and optics

of amblyopes can be completely normal, the effects of visual deprivation or strabismus during development can persist late in life. Vernier acuity deficits in anisotropic amblyopes can be largely accounted for by their resolution deficits. Strabismic amblyopes, however, show greater loss in Vernier acuity than can be predicted by resolution deficits (Levi and Klein, 1982, 1985). Predicting how acuity deficits of strabismics vary with eccentricity is not trivial. There is a lack of temporal-nasal differences in the "good" eye of strabismics (Sireteanu and Fronius, 1981). Nevertheless, the "bad" eye of strabismics demonstrates a nasal bias within the central  $20^\circ$  (Campos, 1995). For both types of amblyopia, we predict a linear relationship between  $M$  and acuity that is shifted relative to that of normals; amblyopes are expected to have higher thresholds overall and lower  $M$  overall at all eccentricities. Whereas there is no expected difference between hemispheres/hemifields in anisotropic amblyopes, there may be a larger  $M$  in the hemisphere contralateral to the bad eye of the strabismic because of the nasal bias in that eye. Both patient populations are in the process of being tested in an ongoing study of ours.

#### Estimating RF Size

Our measurements of  $M$  may be used to predict human receptive field size in V1 by taking advantage of a recently discovered "evolutionary scaling law." Evolutionary scaling relations are generally used to compare the proportional size relationships of structures across species. Recently, Stevens (2001) compared the number of LGN neurons to V1 neurons in 23 haplorhine primates and found that the number of V1 neurons increases as the  $3/2$  power of the number of LGN neurons across species. This relationship holds for the human species; Stevens compared the volumes of V1 and LGN for 24 humans and observed that the volume of V1 was related to LGN volume by the  $3/2$  power. Hence, there is an evolutionary scaling law that governs the proportion of LGN to V1, which may extend to other brain regions as well.

Carrying this evolutionary scaling law one step further, Stevens reasoned that areal cortical magnification factors and RF area might be similarly related (Stevens, 2002). Though it may not seem unreasonable to assume that ACMF and RF size are inversely related, it turns out that RF size increases at a slower rate than would be predicted by the inverse of ACMF, that is, by raising ACMF to the  $-2/3$  power. Unfortunately, fMRI does not allow us to directly measure RF size because the receptive fields corresponding to a given location in visual space are scattered about a mean position in V1 (and vice versa). In our study, RF scatter and RF size are confounded. Even so, we do have a measure of aggregate RF size, which is a combination of RF size and RF scatter ( $4\sqrt{RF_{\text{size}}^2 + RF_{\text{scatter}}^2}$ ) (Dow et al., 1981). Hubel and Wiesel (1974) showed that RF size and scatter are correlated in monkey V1; RF size and scatter increase proportionately with eccentricity, and each factor accounts for approximately half of the aggregate RF size. Assuming that the ratio of RF size to RF scatter is similar in humans, we predict that  $RF_{\text{size}} = \gamma \times \text{ACMF}^{-2/3}$ , where  $\gamma$  is the proportion of  $RF_{\text{size}}$  to  $RF_{\text{aggregate}}$  ( $\gamma = 0.5$ ). After con-

verting our estimates of  $M$  to ACMF, our prediction for RF size in V1 is given by the equation  $RF_{\text{SIZE}} = 0.03 \times \delta^{1.1}$ , where  $\delta$  is eccentricity. Although there is considerable variation in RF size for V1 of different species, the range of our RF size prediction (0.05 to 0.47 deg<sup>2</sup>) for the eccentricities tested is in close agreement with the V1 macaque data collected by others (Hubel and Wiesel, 1974; Van Essen et al., 1984).

### Sources of Error in the Estimation of Cortical Magnification

Since each estimated mapping function between the visual world and each primary visual cortex is a simplified summary of our fMRI data, the mapping function is necessarily imperfect. We chose an oversimplified description of each primary visual cortex because we wanted to capture the gist of each retinotopic map while minimizing contamination of our estimates of cortical magnification by the many sources of noise in the signal and analysis. It is important that these sources of noise do not introduce *systematic* biases into our estimates of cortical magnification. Figure 8 indicates that our estimates of  $M$  are in close agreement with others who used different techniques, suggesting that any systematic error in our measurements is tolerable. Sources of variability in each stage in the process, from visual stimulus to the final estimates of cortical magnification, are described below.

#### *The Visual Stimulus and the Reliability of the Fitting Procedure*

Each flickering ring subtended a finite extent of visual angle. We chose a series of rings whose width was equal to approximately 1/6 of the ring's eccentricity. This width was large enough to produce reliable, robust fMRI responses but thin enough to allow for precise localization of the resulting activity. Due to the nature of  $M$ , the choice of ring width could influence its estimation. For example, increasing the width of the ring an equal distance toward fixation and toward the periphery will expand the region of activation more extensively toward the foveal representation in the cortex than toward the peripheral representation, potentially biasing our estimates of the location of peak activity toward the fovea. The probability that this bias exists increases proportionally with the width of the stimulus. Still, the activity pattern measured using fMRI is actually a combination of two factors: (1) a response localized to the stimulus representation and (2) a spatially diffuse response created by hemodynamic blurring. The hemodynamic blurring is roughly Gaussian and is not spatially biased in a manner that could affect our estimate of  $M$ ; whether the blurring is narrow or broad, the peak of the activity should be the same.

To assess whether our estimates of  $M$  were affected by different stimulus widths and hemodynamic blurring, we conducted two tests. First, we projected the region of visual space occupied by the stimulus onto the flattened representation and compared this projection to the width of the actual activity pattern. As predicted by normal hemodynamic blurring, visual inspection showed that the activity pattern was much larger than the projected stimulus borders. Second, to determine whether activity patterns with different widths affected our esti-

mates of  $M$ , we performed a series of scans where the eccentricity of the stimulus was fixed (6°), but the width was set to 0.5°, 2°, or 6° (1° was used in the original experiment). We fit each pattern of activity using the same fitting protocol described above. The seed for each fit was identical; each fit began from a "mean template" that was computed by averaging the parameters for the five previous fits to each hemisphere from our initial fitting procedure. We found that fits to the activity patterns elicited by these stimuli, with three very different widths, were nearly identical. This lack of variation indicates that our estimates of the peak of activity associated with the actual stimulus representation on the cortex are robust and not easily biased by variations in hemodynamic blurring. Hence, if there is any bias in our estimate of  $M$ , it is too small to significantly affect our conclusions.

In our main experiment, the amount of variability for the projected area is low relative to the change in projected area across eccentricity. This relatively low variability is made evident by the standard error bars in Figure 4, which are typically smaller than the icon. The 95% confidence intervals about the mean projected area (not pictured) range from 0.15 mm at 12° eccentricity to 1.36 mm at 1.5°. Subsequently, according to the function relating  $M$  to Vernier acuity in Figure 5 ( $\tau = 5.97 \times M^{-0.81}$ ), any error associated with estimating the location of a point in visual space from a point on the flattened representation is likely to be off by less than  $\pm 4.6$  min of visual angle at 1.5° eccentricity and  $\pm 27$  min at 12°. Of course, this estimate of error is artificially reduced via statistical averaging, and our ability to predict a position in the visual field from a single voxel on the flattened representation is limited by the voxel size, which is  $3 \times 3 \times 3$  mm. A  $3 \times 3$  mm region on the flattened cortex corresponds to a window of visual space spanning roughly  $0.45^\circ \times 0.45^\circ$  of visual angle at 1.5° eccentricity and  $2.5^\circ \times 2.5^\circ$  of visual angle at 12° eccentricity.

#### *Distortion of Echo-Planar Images*

Magnetic field inhomogeneities produce geometric distortions in echo-planar images that are much less pronounced in T1-weighted anatomical images. This produces a problem for registering functional activity with anatomical images supposedly acquired in the same location (Hutton et al., 2002). These distortions become more problematic with increasing field strength. Our geometric distortions were minimized by the use of a clinical-strength 1.5 T MRI scanner. Also, the signal dropout and spatial distortion that typically results from the sinus and ear cavities was avoided by acquiring coronal images only in the occipital lobe. This resulted in echo-planar images that registered well with T1-weighted images.

#### *Spatial Resolution of fMRI*

One explanation for why our choice of ring widths did not affect our estimates of  $M$  is that the spatial extent of fMRI activation is typically much broader than the underlying neuronal response. By projecting the actual stimulus dimensions onto the flattened cortex, we estimated that the neuronal representation of the ring of activity produced by our annular stimulus was much narrower than the activity patterns of our measured fMRI responses pictured in Figure 2. Thus, while a sufficiently wide stimulus could produce a larger extent of neuronal

activation that could bias our estimate of  $M$ , much of the activity pattern in Figure 2 is due to the blurring of the fMRI response, which is broader in comparison.

The spatial blurring of the fMRI response on the flattened cortex is the result of several factors. First, the hemodynamic changes associated with the BOLD signal are known to extend well beyond the focus of neuronal activation (Grinvald et al., 1994). Second, the spatial sampling of our echo-planar images ( $3 \times 3 \times 3$  mm resolution) will spread the extent of the signal through partial volume effects. Finally, our parameter maps on the flattened representation of the cortex, projected from the in-plane images, were spatially blurred with a Gaussian filter (width at half height =  $1/e$ ). This was done to provide a continuous map with a smooth profile, which facilitated the fitting procedure. These sources of spatial blurring only affect the extent of measured activity, not the location of the peak. Since our conformal map fitting technique searched for the location of peak activity, these sources of spatial blurring should not have introduced a systematic bias in our estimates of cortical magnification.

#### ***Distortions in the Cortical Flattening Technique***

Our estimates of each subject's flattened cortex were obtained through an iterative method that projects the three-dimensional locations of points on the surface of the cortex onto a two-dimensional surface, while minimizing the changes in the pairwise distances between these points (Wandell et al., 2000). Because any region of the surface of the brain will never be perfectly topologically equivalent to a plane, distortions will always be introduced in the cortical flattening process. We minimized distortions by flattening only the smallest region possible because a plane better approximates smaller areas of a smooth curved surface than large areas.

The flattening technique provides an estimate of the amount of distortion in the resulting map, which reflects the remaining amount of stretching or compression at the end of the iteration process. Across all 20 hemispheres, there was an average of approximately  $\pm 10\%$  distortion with a roughly equal amount of compression and expansion. Importantly, we found no systematic pattern of distortion as a function of the representation of eccentricity or polar angle in our flattened maps.

The remaining distortion in our flattened maps is a likely source of noise in our estimates of cortical magnification. This would be particularly troublesome if we were attempting to describe the details of the borders between V1 and V2. However, our method of fitting a smooth template to flattened activity maps keeps local distortions in the flattened representation from producing localized errors in our estimates of cortical magnification.

#### **Experimental Procedures**

##### **Vernier Acuity Task**

Vernier acuity thresholds were measured with four female and six male observers ranging between 21 and 34 years of age. Observers sat in a quiet, light-controlled room (ambient luminance  $< 1$  cd/m<sup>2</sup>) 57.3 cm from the display monitor with their heads stabilized in a chin rest. Stimuli were viewed binocularly through natural pupils. An Apple Power Mac computer controlled stimulus presentation and data acquisition (PowerMac G3 processor; 300 MHz; 8 bit graphics

control card;  $1024 \times 768$  pixels; 60 Hz) using Matlab 5.2 software with the Psychophysics Toolbox (Brainard, 1997; Pelli, 1997). Stimuli were displayed on a 53 cm analog RGB video monitor (Sony Multiscan 500 PS) with each pixel subtending 1.67 min of visual angle. For the most foveal stimulus ( $1.5^\circ$  eccentricity), the stimulus presentation and data acquisition were controlled by an Apple PowerBook laptop computer (PowerMac G3 processor; 300 MHz; 8 bit graphics control card;  $1024 \times 768$  pixels; 75 Hz) and displayed on a 43 cm analog RGB video monitor (Sony Multiscan 200 PS) at a viewing distance of 230 cm. At that viewing distance, each pixel subtended 0.43 min of visual angle. Stimuli consisted of two white, vertical lines presented one above the other on a black background. Each line measured 5 min by  $1^\circ$  of visual angle and the two lines were separated vertically by 10 min of visual angle. The midpoint of each line pair fell at a distance of  $1.5^\circ$ ,  $3^\circ$ ,  $6^\circ$ ,  $9^\circ$ , or  $12^\circ$  from a central fixation target measuring 15 by 15 min visual angle. All stimuli had the same screen dimensions except when viewed at  $1.5^\circ$  eccentricity, during which all aspects of the stimulus were scaled to match the change in viewing distance. Thresholds were acquired using a two-interval forced-choice paradigm and a staircase procedure. For each trial, two pairs of stimuli were presented at a particular eccentricity in succession. Pairs of stimuli consisted of one set of colinear lines and one set of horizontally offset lines. Horizontal offsets were created by displacing each of the lines an equal distance from their mean horizontal position. The direction of displacement about the mean position was randomized from trial to trial. The temporal interval that contained the offset line pairs was also randomized. The observers' task was to indicate which of the two temporal intervals contained the pair of lines that were horizontally offset. Observers reported their decision by pressing one of two buttons on a computer keyboard. Each pair of lines was presented for 1000 ms and separated by an interval of 500 ms. Observers were given 2000 ms at the end of each trial to respond. The intertrial interval was always 500 ms. Horizontal offsets between lines were determined using a staircase procedure. Horizontal offsets were decreased after three correct answers in a row and increased after one incorrect answer. Each staircase contained 80 trials. To reach threshold in a shorter number of trials, the increment by which offsets were adjusted was larger by one and two orders of magnitude for the first 20 and 40 trials, respectively. Vernier stimuli were presented at five eccentricities in all four quadrants (up-left, up-right, down-left, and down-right) for four repetitions, yielding a total of 6400 trials per observer. For a given session, the data from the staircase (80 trials) were combined and fit with a Weibull function using a maximum likelihood procedure to compute the threshold (79% correct) for that condition. The few sessions that did not yield acceptable fits were removed from the analysis and repeated. Thresholds were then averaged across repetitions and quadrants to obtain a mean threshold at each eccentricity for the left and right hemifield of each observer.

##### **Grating Resolution Task**

Grating resolution was measured using the laser interferometry device in the laboratory of Donald MacLeod in the University of California at San Diego's department of Psychology. The same ten observers were seated in complete darkness, and their heads were stabilized with a dental bite bar. Observers wore an eye patch over one eye and viewed the stimulus through the unoccluded eye. Stimuli were viewed through natural pupils and were composed of horizontal gratings with spatial frequencies ranging between 5 to 75 cycles/° circumscribed within a  $1^\circ$  aperture. The mean luminance of the stimulus was  $\sim 1000$  trolands. The red laser-generated stimulus was presented on a dim background of green-filtered light by combining the paths of each light source with a beam splitter. Observers fixated a  $0.1^\circ$  diameter fixation target that was created by printing a spot on acetate and placing the acetate in the path of the background illumination. Observers were asked to determine whether the grating was oriented  $15^\circ$  clockwise or counterclockwise from horizontal. Grating presentation was preceded by a tone. After the grating was presented (1000 ms), observers indicated their response using a key press (two-alternative forced choice). The grating orientation was randomized from trial to trial, and the spatial frequency of the grating was determined using a staircase procedure. The spatial frequency of the grating was increased for every three correct

trials and decreased for every incorrect trial. We randomly interleaved two staircases during each run (50 trials each). The data for each session was combined and fit with a Weibull function to determine thresholds (~79% correct). The thresholds corresponding to the temporal retina of one eye were averaged with the nasal thresholds of the other eye (and vice versa) to obtain a mean threshold for the left and right visual hemifields.

#### General fMRI Methodology

fMRI images were acquired at Thornton Hospital at the University of California at San Diego using a 1.5 Tesla Siemens VISION system scanner. The controlling computer used Numaris 3 software with full echo-planar imaging (EPI) capabilities, including the EPI booster. Two high-resolution anatomical scans were collected with a volume head coil and averaged to provide a three-dimensional reference volume for each observer. We used a small flex coil (approximately 15 × 30 cm) in our functional scans to maximize the signal-to-noise ratio over the occipital lobe. Observers lay on their backs in the bore of the scanner and looked directly up into an angled mirror to view a projection screen positioned near their neck. Care was taken to assure that viewing distance was consistent between observers and sessions (18 cm). A bite bar was used to stabilize the heads of the observers. Visual stimuli were back projected onto the screen using the aforementioned software, laptop computer, and a Proxima DP9300 LCD video projector (max brightness = 1500 lumens; resolution = 1024 × 768; 60 Hz) equipped with a specialized lens. Each pixel of the projector subtended 4.05 min of visual arc. During each functional scan, 130 temporal frames were acquired using a low-bandwidth EPI pulse sequence lasting 260 s (TR = 2 s, flip angle = 70°, 16 slices of 3 mm thickness and 3 × 3 mm resolution, FOV = 192 mm). The first ten temporal frames (20 s) were discarded to avoid magnetic saturation effects. Up to ten scans were acquired from each observer during each scanning session. Each session contained two repetitions of each condition from a given experiment. Each scanning session ended with an anatomical scan using a standard T1-weighted gradient echo pulse sequence (MPRAGE, 1 × 1 × 1 mm resolution). Anatomical scans were used to align functional data across multiple scanning sessions to an observer's reference volume. The stimulus presentation was synchronized with fMRI data acquisition using a custom-made trigger.

#### Standard Retinotopy

For our basic retinotopy experiments, stimuli consisted of expanding rings and rotating wedges made from flickering black and white checkerboard patterns (8 Hz counterphase flicker; mean luminance = 340 cd/m<sup>2</sup>; contrast = 100%). Stimuli were presented on a mean gray background. The width of the expanding rings was roughly 1/6 of the eccentricity, and the polar angle of the wedges was 45°. Expanding rings and rotating wedges were presented for 6 1/2 cycles of 40 s each. Data from the first 1/2 cycle was discarded to avoid magnetic saturation effects. In addition to the rings and wedges, we mapped the horizontal and vertical meridians using alternating "hourglass" and "bow tie" shaped checkerboard patterns. Meridian mapping stimuli were composed of two mirror-symmetric, triangular subregions spanning 90° of polar angle about the meridian. Meridian mapping stimuli were alternated every 20 s for 6 1/2 40 s cycles (including the discarded 1/2 cycle). Occipital visual areas V1, V2, V3, V4, and V3A were defined using standard retinotopy and cortical-flattening techniques (Boynton et al., 1999; Engel et al., 1994; Sereno et al., 1995). First, gray matter was identified in the high-resolution reference volume using a Bayesian classification algorithm (Teo et al., 1997). Next, a multidimensional scaling algorithm was used to computationally flatten the occipital lobe of each hemisphere (Engel et al., 1997). Software for both gray matter segmentation and cortical flattening is available online at <http://white.stanford.edu>. Each functional scan was then aligned to the reference volume and projected onto the flattened representation of cortex using the following procedure. First, corresponding locations between the in-plane anatomies for each functional scan and the reference volume were identified by eye. Second, in-plane anatomies were aligned with the reference volume by finding the optimal translation and rotation between the two sets of points (Arun et al., 1987). Third, fMRI measurements were then projected onto the flattened

representation via the reference volume. Some points on the flattened representation are not covered with a functional measurement. Consequently, the functional data were interpolated using a blurring algorithm; each pixel on the flattened representation was assigned a weighted average of the neighboring pixels that contained functional data. After the retinotopy was projected on the cortex, the boundaries of visual areas were delineated by hand. Typically, there is only 2–4 mm of error associated with this technique (Engel et al., 1997). Finally, after the borders of V1 were identified, a smaller area of the cortex around V1 was reflattened to minimize any distortions created by flattening.

#### Acknowledgments

We would like to thank Ione Fine, Ed Hubbard, Melissa Saenz, Chuck Stevens, and August Tuan for helpful comments on drafts of this manuscript. Additionally, we thank Don MacLeod and Sherif Shady for use of the interferometer and associated software. Supported by National Institutes of Health grants EY07028-02 and EY12925.

Received: August 8, 2002

Revised: February 11, 2003

Accepted: March 3, 2003

Published: May 21, 2003

#### References

- Arun, K.S., Huang, T.S., and Blotstein, S.D. (1987). Least-squares fitting of two 3-d point sets. *IEEE PAMI* 9, 698–700.
- Azzopardi, P., and Cowey, A. (1993). Preferential representation of the fovea in the primary visual cortex. *Nature* 361, 719–721.
- Beard, B.L., Levi, D.M., and Klein, S.A. (1997). Vernier acuity with non-simultaneous targets: the cortical magnification factor estimated by psychophysics. *Vision Res.* 37, 325–346.
- Boynton, G.M., Demb, J.B., Glover, G.H., and Heeger, D.J. (1999). Neuronal basis of contrast discrimination. *Vision Res.* 39, 257–269.
- Brainard, D.H. (1997). The psychophysics toolbox. *Spat. Vis.* 10, 433–436.
- Brindley, G.S., and Lewin, W.S. (1968). The sensations produced by electrical stimulation of the visual cortex. *J. Physiol.* 196, 479–493.
- Campos, E. (1995). Amblyopia. *Surv. Ophthalmol.* 40, 23–39.
- Coletta, N.J., and Williams, D.R. (1987). Psychophysical estimate of extrafoveal cone spacing. *J. Opt. Soc. Am. A* 4, 1503–1513.
- Connolly, M., and Van Essen, D. (1984). The representation of the visual field in parvocellular and magnocellular layers of the lateral geniculate nucleus in the macaque monkey. *J. Comp. Neurol.* 226, 544–564.
- Cowey, A., and Rolls, E.T. (1974). Human cortical magnification factor and its relation to visual acuity. *Exp. Brain Res.* 21, 447–454.
- Curcio, C.A., and Allen, K.A. (1990). Topography of ganglion cells in human retina. *J. Comp. Neurol.* 300, 5–25.
- Curcio, C.A., Sloan, K.R., Jr., Packer, O., Hendrickson, A.E., and Kalina, R.E. (1987). Distribution of cones in human and monkey retina: individual variability and radial asymmetry. *Science* 236, 579–582.
- Daniel, P.M., and Whitteridge, D. (1961). The representation of the visual field on the cerebral cortex in monkeys. *J. Physiol.* 159, 203–221.
- Dow, B.M., Snyder, A.Z., Vautin, R.G., and Bauer, R. (1981). Magnification factor and receptive field size in foveal striate cortex of the monkey. *Exp. Brain Res.* 44, 213–228.
- Engel, S.A., Rumelhart, D.E., Wandell, B.A., Lee, A.T., Glover, G.H., Chichilnisky, E.J., and Shadlen, M.N. (1994). fMRI of human visual cortex. *Nature* 369, 525.
- Engel, S.A., Glover, G.H., and Wandell, B.A. (1997). Retinotopic organization in human visual cortex and the spatial precision of functional MRI. *Cereb. Cortex* 7, 181–192.
- Fahle, M., and Schmid, M. (1988). Naso-temporal asymmetry of visual perception and of the visual cortex. *Vision Res.* 28, 293–300.

- Filimonoff, I.N. (1932). Über die variabilität der grosshirnrindenstruktur. Mitteilung II. Regio occipitalis beim erwachsenen Menschchen. *J. Psychol. Neurol.* *44*, 1–96.
- Grinvald, A., Lieke, E.E., Frostig, R.D., and Hildesheim, R. (1994). Cortical point-spread function and long-range lateral interactions revealed by real-time optical imaging of macaque monkey primary visual cortex. *J. Neurosci.* *14*, 2545–2568.
- Grusser, O.J. (1995). Migraine phosphenes and the retino-cortical magnification factor. *Vision Res.* *35*, 1125–1134.
- He, S., and MacLeod, D.I. (1996). Local luminance nonlinearity and receptor aliasing in the detection of high-frequency gratings. *J. Opt. Soc. Am. A* *13*, 1139–1151.
- Hubel, D.H., and Wiesel, T.N. (1974). Uniformity of monkey striate cortex: a parallel relationship between field size, scatter, and magnification factor. *J. Comp. Neurol.* *158*, 295–305.
- Hutton, C., Bork, A., Josephs, O., Deichmann, R., Ashburner, J., and Turner, R. (2002). Image Distortion Correction in fMRI: A Quantitative Evaluation. *Neuroimage* *16*, 217–240.
- Kerr, J.L. (1971). Visual resolution in the periphery. *Percept. Psychophys.* *9*, 375–378.
- Levi, D.M., and Klein, S. (1982). Differences in vernier discrimination for grating between strabismic and anisometric amblyopes. *Invest. Ophthalmol. Vis. Sci.* *23*, 398–407.
- Levi, D.M., and Klein, S.A. (1985). Vernier acuity, crowding and amblyopia. *Vision Res.* *25*, 979–991.
- Levi, D.M., Klein, S.A., and Aitsebaomo, P. (1984). Detection and discrimination of the direction of motion in central and peripheral vision of normal and amblyopic observers. *Vision Res.* *24*, 789–800.
- Levi, D.M., Klein, S.A., and Aitsebaomo, A.P. (1985). Vernier acuity, crowding and cortical magnification. *Vision Res.* *25*, 963–977.
- Levi, D.M., McGraw, P.V., and Klein, S.A. (2000). Vernier and contrast discrimination in central and peripheral vision. *Vision Res.* *40*, 973–988.
- Pelli, D.G. (1997). The VideoToolbox software for visual psychophysics: transforming numbers into movies. *Spat. Vis.* *10*, 437–442.
- Popovic, Z., and Sjostrand, J. (2001). Resolution, separation of retinal ganglion cells, and cortical magnification in humans. *Vision Res.* *41*, 1313–1319.
- Rockel, A.J., Hiorns, R.W., and Powell, T.P. (1980). The basic uniformity in structure of the neocortex. *Brain* *103*, 221–244.
- Rolls, E.T., and Cowey, A. (1970). Topography of the retina and striate cortex and its relationship to visual acuity in rhesus monkeys and squirrel monkeys. *Exp. Brain Res.* *10*, 298–310.
- Rovamo, J., Virsu, V., and Nasanen, R. (1978). Cortical magnification factor predicts the photopic contrast sensitivity of peripheral vision. *Nature* *271*, 54–56.
- Schwartz, E.L. (1980). Computational anatomy and functional architecture of striate cortex: a spatial mapping approach to perceptual coding. *Vision Res.* *20*, 645–669.
- Schwartz, E.L. (1994). Computational studies of the spatial architecture of primate visual cortex. In *Cerebral Cortex*, A. Peters and K.S. Rockland, eds. (New York: Plenum Press), pp. 359–411.
- Sereno, M.I., Dale, A.M., Reppas, J.B., Kwong, K.K., Belliveau, J.W., Brady, T.J., Rosen, B.R., and Tootell, R.B. (1995). Borders of multiple visual areas in humans revealed by functional magnetic resonance imaging. *Science* *268*, 889–893.
- Sholl, D.A. (1956). *The Organization of the Cerebral Cortex* (London: Methuen).
- Sireteanu, R., and Fronius, M. (1981). Naso-temporal asymmetries in human amblyopia consequence of long-term interocular suppression. *Vision Res.* *21*, 1055–1063.
- Smith, A.T., Singh, K.D., Williams, A.L., and Greenlee, M.W. (2001). Estimating receptive field size from fMRI data in human striate and extrastriate visual cortex. *Cereb. Cortex* *11*, 1182–1190.
- Stensaas, S.S., Eddington, D.K., and Dobbelle, W.H. (1974). The topography and variability of the primary visual cortex in man. *J. Neurosurg.* *40*, 747–755.
- Stevens, C.F. (2001). An evolutionary scaling law for the primate visual system and its basis in cortical function. *Nature* *411*, 193–195.
- Stevens, C.F. (2002). Predicting functional properties of visual cortex from an evolutionary scaling law. *Neuron* *36*, 139–142.
- Teo, P.C., Sapiro, G., and Wandell, B.A. (1997). Creating connected representations of cortical gray matter for functional MRI visualization. *IEEE Trans. Med. Imaging* *16*, 852–863.
- Thibos, L.N., Cheney, F.E., and Walsh, D.J. (1987). Retinal limits to the detection and resolution of gratings. *J. Opt. Soc. Am. A* *4*, 1524–1529.
- Tootell, R.B., Silverman, M.S., Switkes, E., and De Valois, R.L. (1982). Deoxyglucose analysis of retinotopic organization in primate striate cortex. *Science* *218*, 902–904.
- Van Essen, D.C., Newsome, W.T., and Maunsell, J.H. (1984). The visual field representation in striate cortex of the macaque monkey: asymmetries, anisotropies, and individual variability. *Vision Res.* *24*, 429–448.
- Wandell, B.A., Chial, S., and Backus, B.T. (2000). Visualization and measurement of the cortical surface. *J. Cogn. Neurosci.* *12*, 739–752.
- Wertheim, T. (1894). Über die indirekte schescharefe. *Z Psychol. Physiol. Sinnesorg* *7*, 172–189.
- Westheimer, G. (1982). The spatial grain of the perifoveal visual field. *Vision Res.* *22*, 157–162.
- Weymouth, F.W., Hines, D.C., Acres, L.H., Raaf, J.E., and Wheeler, M.C. (1928). Visual acuity within the area centralis and its relation to eye movements and fixation. *Am. J. Ophthalmol.* *11*, 947–960.
- Whitaker, D., Rovamo, J., MacVeigh, D., and Makela, P. (1992). Spatial scaling of vernier acuity tasks. *Vision Res.* *32*, 1481–1491.
- Wilhelm, H., and Fahle, M. (1993). Lack of naso-temporal asymmetry in the central visual field of normal subjects. *Clin. Vis. Sci.* *8*, 609–612.